Rheol Acta (2006) 45: 677–692
DOI 10.1007/s00397-005-0026-6

ORIGINAL CONTRIBUTION

Davide Valtorta
Edoardo Mazza

Measurement of rheological properties of soft biological tissue with a novel torsional resonator device

Received: 11 October 2004
Accepted: 21 July 2005
Published online: 13 September 2005

D. Valtorta (✉) · E. Mazza
Institute of Mechanical Systems, ETH Zurich, 8092 Zurich, Switzerland
E-mail: valtorta@imes.mavt.ethz.ch

Abstract A new device for measuring the rheological properties of soft biological tissues is presented. The mechanical response is characterized for harmonic shear deformations at high frequencies (up to 10 kHz) and small strains (up to 0.2%). Experiments are performed using a cylindrical rod excited to torsional resonance. One extremity of the rod is in contact with the soft tissue and adherence is ensured by vacuum clamping. The damping characteristics and the resonance frequency of the vibrating system are inferred from the control variables of a phase stabilization loop. Due to the contact with the soft tissue, and depending on the rheological properties of the tissue, changes occur in the Q-factor and in the resonance frequency of the system. The shear modulus of the soft tissue is determined from the experimental results with an analytical model. The reliability of the proposed technique is evaluated through repeatability tests and comparative measurements with synthetic materials. The results of measurements on bovine organs demonstrate the suitability of the experimental procedure for the characterization of biological tissues and provide some insight in their rheological properties at frequencies in the range 1–10 kHz.

Introduction

The identification of the mechanical properties of soft biological tissues is essential to a number of medical applications, such as for diagnostic purposes, surgery planning and training of surgical procedures with virtual reality-based simulators (Avis 2000; Greenleaf et al. 2003; Picinbono et al. 2002; Szekely 2003)

Different approaches have been proposed for quasi-static and dynamic testing of soft biological tissue. Quasi-static experiments typically provide information on the nonlinear viscoelastic response for large deformations at low-deformation rates, which is useful for prediction of organ deformations under physiological loads or simulation of surgical procedures. A number of different procedures for quasi-static tissue testing have been recently developed. They are based on indentation, aspiration or shear testing (Hendriks et al. 2003; Kauer et al. 2002; Miller et al. 2000; Nava et al. 2004; Ottensmeyer 2002; Zheng and Mak 1996)

Dynamic testing at higher strain rates provides additional information on the constitutive behavior of the tissue, with applications in diagnostics and trauma research (Snedeker et al. 2005). Methods for dynamically testing soft biological materials range from standard rheometers operating at 0.01 to 10 Hz (Liu and Bilston 2000; Nasseri et al. 2002), to devices suitable for characterization up to 350 Hz (Arbogast et al. 1997). Techniques suitable for in vivo measurements offer the great advantage of a characterization in the natural biochemical environment with blood supply and hormone stimuli, which influence the mechanical properties of the tissue in a significant way. In the work of Kruse et al. (2000), Manduca et al. (2001), porcine tissues were tested ex vivo and in vivo from 50 to 300 Hz. Rotary shear tests have been proposed for in vivo tests by

Kalanovic et al. (2003) for the low-frequency range (up to 20 Hz).

A novel method for dynamic testing of soft tissues is presented in this paper. The mechanical properties are derived from the material response to harmonic shear at high frequencies (1–10 kHz) and small strains (up to 0.2%). The experimental set-up consists of a cylindrical rod excited to torsional resonance. One extremity of the rod adheres to a tissue sample so that the dynamic behavior of the system rod + tissue depends on the rheological properties of the tissue sample.

Use of oscillating probes for the characterization of the rheological properties at high frequencies has been previously proposed for fluid films by Sayir et al. (1995) and Romoscanu et al. (2003). There, the dynamic behavior of the system oscillator + fluid film in the

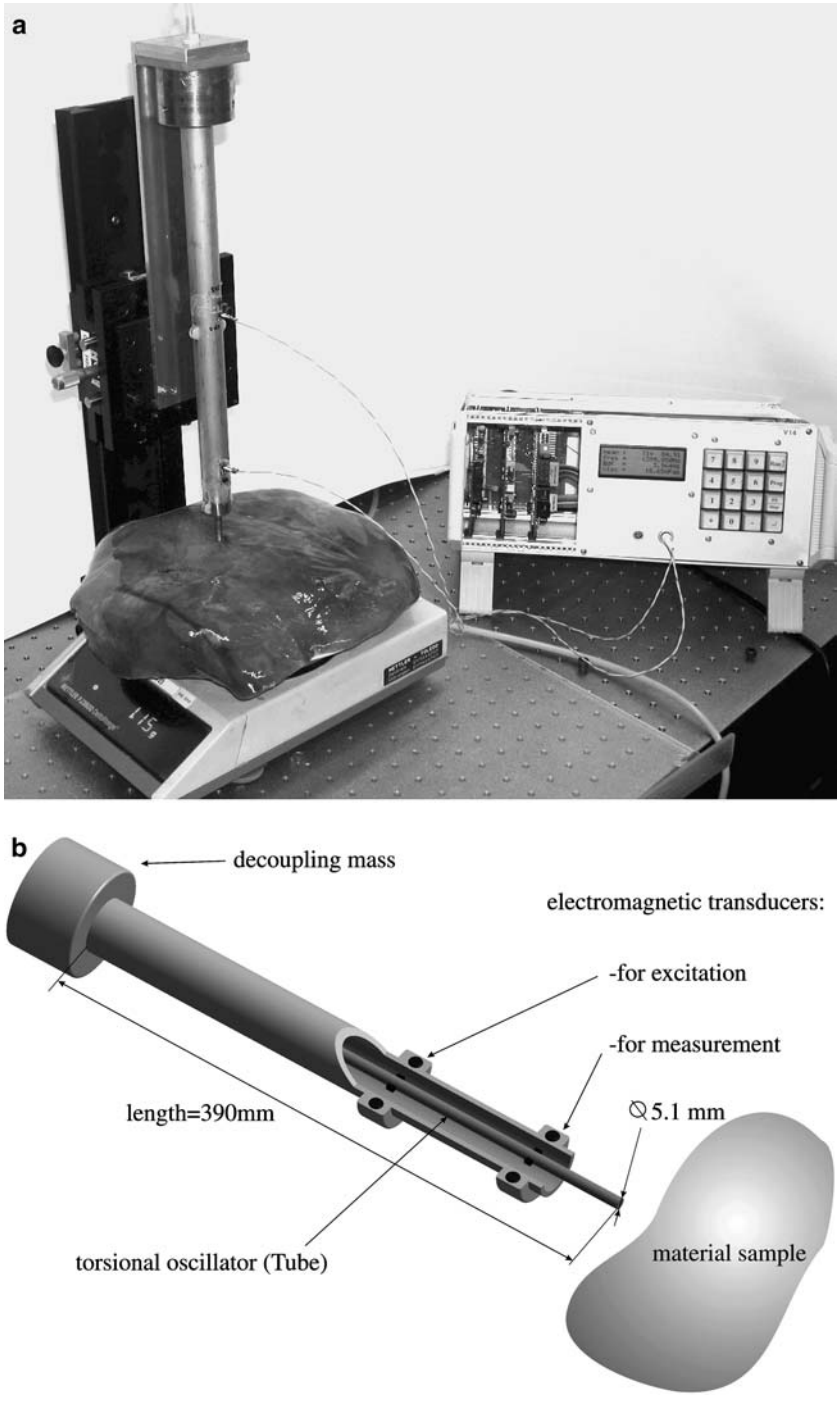

Fig. 1 Torsional Resonator Device (TRD): photograph (*above*) and sketch (*below*)

vicinity of its resonance frequency are precisely characterized from the phase curve of the system transfer function using a phase locked loop algorithm. A mechanical model allows determining the complex viscosity of the fluid from the resonance frequency and the damping characteristics of the resonator. Here, we use the same measurement principle for characterizing the complex shear modulus of soft biological tissue, using a novel torsional resonator device (TRD). Complex shear modulus is derived from the experimental results using the analytical model of a torsional radiating source on a semi-infinite space (Sagoci 1944; Sneddon 1966; Robertson 1967; Dorn 1980). Thereby, the soft tissue is modeled as linear viscoelastic, homogenous and isotropic.

The present non-destructive technique is designed for in vivo application and complements our quasi-static tissue characterization with aspiration experiments (Nava et al. 2003). The measurement is fast and, due to the small contact area, a local characterization is achieved. A mapping procedure and reference tables enable very fast (almost "on-line") determination of material parameters. Our technique does not require specific sample preparation, can be applied to samples of virtually arbitrary shape and uses simple, portable and inexpensive components. These characteristics make it attractive not only for characterization of biological tissues but also for soft synthetic materials.

The experimental set-up is presented here along with the analytical model for material parameters evaluation. The procedure is validated with measurements on soft synthetic materials, for which viscoelastic properties were also measured with wave propagation experiments. Results of measurements on bovine soft organs (liver, kidney, uterus) are reported and the characteristics of this new technique are discussed.

Experiment

The Torsional Resonator Device, Fig. 1, consists of a cylinder made of brass. It is excited around one of the first five torsional eigenfrequencies (in the range of 1–10 kHz) by an electromagnetic transducer, while a second electromagnetic transducer is used as sensor for measuring the motion. The cylinder is clamped at one extremity with a decoupling mass. The other extremity is free for the so-called "calibration run", and is in contact with the tissue sample for the "measurement run". The tissue sample lays on a balance, used for ensuring that no axial forces are exerted on the tissue (resolution 10^{-1} mN).

Equation 1 defines the complex transfer function of the system $T^*(f)$ (being f frequency) as the ratio between the resulting motion of the tube $\theta(f,\ t) = \theta_0^* e^{j2\pi ft}$ and the exciting torque $M(f,\ t) = M_0^* e^{j2\pi ft}$:

$$T^*(f) = \frac{\theta(f,t)}{M(f,t)} \tag{1}$$

Significant changes in the dynamic behavior of the vibrating system occur as the free end of the resonator adheres to the soft material. Figure 2 shows the typical transfer function of the system, vibrating at resonance during a calibration run and a measurement run. Two parameters, that can be evaluated from the phase curve ($\mathrm{Arg}(T^*(f))$), characterize the dynamic behavior of the system: the resonance frequency f_{res}, and the quality factor Q. The quality factor is defined in Eq. 2 and is proportional to the ratio of maximum potential energy stored in the vibrating structure U_{m} and the energy loss due to damping in one vibration period D:

$$Q = \frac{2\pi U_{\mathrm{m}}}{D} \tag{2}$$

Q can be determined from the phase curve in the vicinity of resonance (Bert 1973; Bishop and Johnson 1979), as in Eq. 3

$$Q = \frac{f_{\mathrm{res}}}{df} \tag{3}$$

$$df = f^+\left(\phi = \frac{\pi}{2} + \frac{\pi}{4}\right) - f^-\left(\phi = \frac{\pi}{2} - \frac{\pi}{4}\right) \tag{4}$$

where the two measured frequencies f^+ and f^- (see Fig. 2) correspond to a phase shift difference $\Delta\phi = \pm\pi/4$ with respect to the resonance frequency f_{res} (where $\phi = \pi/2$). The damping characteristic (df) and the resonance frequency (f_{res}) are inferred from the control variables of a phase stabilization loop, using a technique employed in viscosimetry by Sayir et al. (1995) and Romoscanu et al. (2003). Figure 3 illustrates the phase

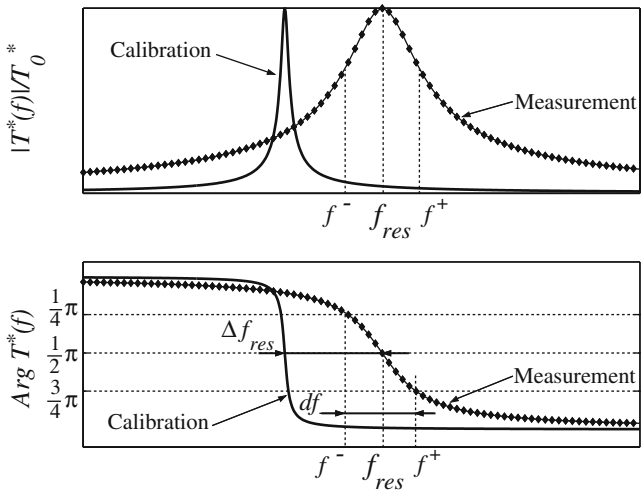

Fig. 2 Transfer functions of the vibrating system. Comparison between a calibration run (TRD in air) and a measurement run (TRD in contact with tissue)

locked loop algorithm: the excitation frequency is adjusted (using a PI controller) in two subsequent steps in order to achieve the prescribed phase difference between excitation and motion around resonance ($\pi/2+\pi/4$ and $\pi/2-\pi/4$). The damping characteristics (df) is determined from the corresponding values of excitation frequency as in Eq. 4, and the Q factor is calculated according to Eq. 3. The control loop allows stabilizing the system so to ensure high accuracy in the determination of f_{res} and df (Sayir et al. 1995).

The Q factor of the calibration run is typically in the range of 30,000, corresponding to a system with very low damping, whereas the measurement run typically exhibits Q factors lower than 3,000. For the evaluation of the rheological properties of the tissue sample the specific damping of the torsional resonator is therefore neglected. The experimental results used for the evaluation of tissue properties are: (1) the change in resonance frequency between calibration and measurement run Δf_{res}, and (2) the quality factor Q from the measurement run.

The contact area with the material sample (Fig. 4) at the lower extremity of the resonator has a radius $R = 2.55$ mm. Since perfect adherence will be assumed in the analytical model for parameter extraction, any sliding between the resonator and the soft tissue sample must be avoided. Therefore, a single crystal silicon disc with micro-openings, as shown in Fig. 4, is bonded at the extremity of the resonator. The disc has been manufactured from silicon wafers using high-precision microfabrication technologies. The cylinder is indeed a tube with controllable internal pressure. By evacuating the internal volume of the tube, adherence between resonator and soft tissues is obtained (vacuum clamping).

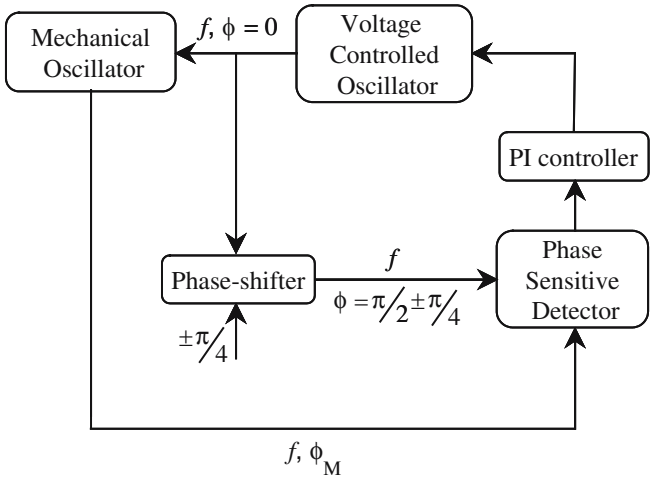

Fig. 3 Phase stabilization algorithm

Due to the small dimensions of the disc openings (width = 30 μm, Fig. 4) and the low underpressure applied in the tube (0.2 bar absolute pressure) no damage occurs in the tissue as a consequence of vacuum clamping. Absence of bleeding, lacerations and abrasions were verified by visual inspection after testing biological tissue samples. The vibration amplitude is kept below 0.001 rad, therefore limiting the shear strains to $\gamma_{max} < 0.2\%$, for the materials and range of frequencies considered here. In agreement with the results found by Liu and Bilston (2000) and Nasseri et al. (2002), at this strain amplitude tissue response is assumed to be linear viscoelastic.

A typical experimental procedure with TRD consists of the following steps: (1) a calibration run is performed; (2) the resonator is put in contact with the material sample, and the internal pressure of the tube is decreased; (3) a measurement run is performed. The whole procedure takes approximately 1 min, and can be repeated for the first five torsional eigenfrequencies of the resonator. At the characteristic frequencies of these experiments, the observation time leads to several thousand oscillations periods, so that a steady harmonic response state is reached in the system.

Analytical model

Characterization of the rheological properties of a tissue, in terms of frequency dependent complex shear modulus or complex viscosity, can be obtained from this experiment only for homogeneous and isotropic tissues. In fact, inhomogeneities (e.g., a layered tissue) or anisotropy (in the plane of the tissue surface and perpendicular to it) lead to a larger number of material and geometry parameters which cannot be uniquely determined from the two experimental data Δf_{res} and Q.

An analytical model is presented here to link the frequency dependent complex shear modulus (consisting of two components: storage and loss modulus) to the experimental data Δf_{res} and Q. With reference to Fig. 5, the tissue is modeled as a semi-infinite viscoelastic space. A cylindrical coordinate system (r, φ, z) is used. The torsional resonator is in contact with the tissue surface, vibrates around the z-axis and excites shear waves with displacement in the r-φ plane (SH-waves) in the tissue. Linear viscoelasticity is assumed to describe the tissue behavior in shear deformation:

$$\tau(t) = \left(G(0) + \int_0^\infty e^{-j\omega s} \dot{G}(s) ds \right) \cdot \gamma(t) = G^* \gamma(t) \qquad (5)$$

$$\gamma(t) = \gamma_0 e^{j\omega t} \qquad (6)$$

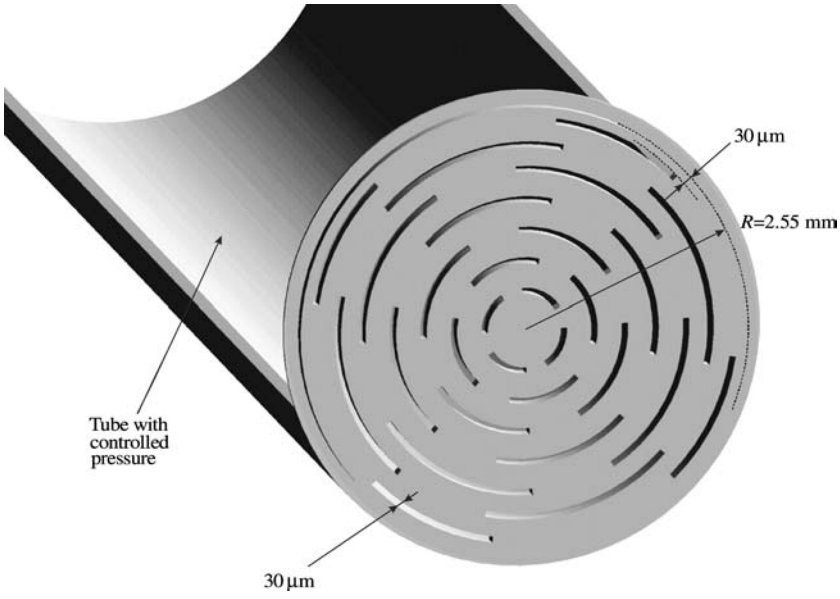

Fig. 4 A disc with micro-openings is bonded at the lower extremity of the TRD: this ensures adherence through vacuum clamping

$$G^* = G_1 + jG_2 = |G^*|e^{j\delta}; \quad \delta = \arctan\frac{G_2}{G_1} \tag{7}$$

where $\tau(t)$ and $\gamma(t)$ represent the shear stress and strains, respectively, and ω is the angular frequency of their harmonic time function. G^* is the complex shear modulus of the material, with the real and imaginary components G_1 and G_2, called respectively storage and loss shear modulus. In the equivalent exponential notation, $|G^*|$ represents the moduli and δ the phase. Due to the kinematic boundary condition at the tissue surface, the displacement vector field in the half space can be described as in Eq. 8, thus reducing to the azimuthal component u_φ only:

$$\mathbf{u} = u_r\hat{r} + u_\varphi\hat{\varphi} + u_z\hat{z} = u_\varphi\hat{\varphi} = u_\varphi(r,z,t)\hat{\varphi}, \quad u_r = u_z = 0 \tag{8}$$

Considering from now on, for simplicity, the displacement $u_\varphi = u$ and assuming a time-harmonic displacement $u(r, z, t) = u(r, z)e^{j\omega t}$, the equations of linear momentum and the kinematic relations lead here to the SH-wave equation in a viscoelastic half space (Eq. 9), where c_{SH} identifies the complex shear wave speed in the material of density ρ:

$$\frac{\partial^2 u}{\partial z^2} + \frac{\partial}{\partial r}\left[\frac{1}{r}\frac{\partial(ru)}{\partial r}\right] + \frac{\omega^2}{c_{SH}^2}u = 0, \quad c_{SH}^2 = \frac{G^*}{\rho} \tag{9}$$

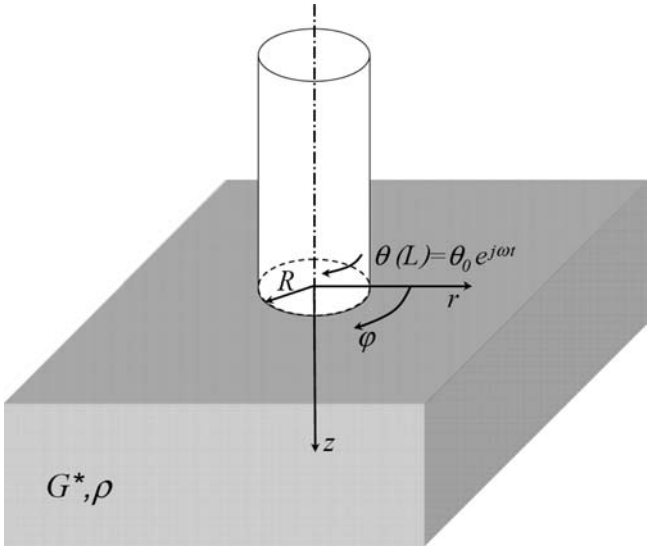

Fig. 5 Half-space model of the tissue with cylindrical coordinate system

The problem of a torsional radiating source on a viscoelastic half space, first studied by Reissner and Sagoci (1944), then treated also by Sneddon (1966) and Robertson (1967), can be solved by specifying either a stress distribution or a displacement field in the contact area of radius R, as shown in Fig. 5. In this study, we assume perfect adherence in the contact region, which is obtained experimentally by vacuum clamping, so that the boundary conditions are:

$$u_{|z=0} = \theta_0 r e^{j\omega t} \quad \text{for } 0 < r \le R \tag{10}$$

$$\tau_{\varphi z|z=0} = 0 \quad \text{for } r > R \tag{11}$$

which identify a linear displacement field in the contact area and a stress-free surface outside the contact area.

The solution of this boundary value problem with mixed (kinematic and kinetic) boundary conditions can

be obtained using the method described by Dorn (1980). The problem is solved here with a dimensionless approach (the subscript 0 indicates dimensionless quantities), dividing all distances by the radius R of the contact area. Equation 9 is rewritten in the following form:

$$\frac{\partial^2 u_0}{\partial z_0^2}+\frac{\partial}{\partial r_0}\left[\frac{1}{r_0}\frac{\partial (r u_0)}{\partial r_0}\right]+k_0^2 u_0=0, \quad k_0=\frac{\omega}{c_{\mathrm{SH}}}R \tag{12}$$

where k_0 is the dimensionless wave number. This number characterizes the wave propagation pattern in the half space and will be further discussed. The relation between the shear stress and the displacement gradient in the contact area,

$$\tau_{\varphi z}(r,0)=G^*\frac{\partial u(r,0)}{\partial z} \tag{13}$$

can be rewritten by defining a dimensionless stress $\tau_{0\varphi z}=\tau_{\varphi z}/G^*$ as follows

$$\tau_{0\varphi z}(r_0,0)=\frac{\partial u_0(r_0,0)}{\partial z_0} \tag{14}$$

The solution of the Bessel-type differential equation 12 can be obtained using the Hankel transform (Abramowitz and Stegun 1972), defined in Eq. 15

$$\bar{f}(\xi,z)=\mathbf{H}_1[f(r,z);\xi]=\int_0^\infty f(r,z) r \mathbf{J}_1(\xi r)\mathrm{d}r \tag{15}$$

where $\mathbf{J}_1$ is the Bessel function of first kind of the new Hankel-transformed variable ξ, which substitutes r. Functions with the bar symbol $\bar{f}$ will be now defined in the Hankel space. Applying the $\mathbf{H}_1$ transform to Eq. 12, the elastodynamic wave equation can be simplified as

$$\bar{u}_0(\xi_0,z_0)=\mathbf{H}_1[u_0(r_0,z_0);\xi_0] \tag{16}$$

$$\frac{\mathrm{d}^2\bar{u}_0}{\mathrm{d}z_0^2}+(k_0^2-\xi_0^2)\bar{u}_0=0 \tag{17}$$

The solution of Eq. 17, for a wave traveling toward the half space interior, can be expressed as

$$\bar{u}_0(\xi_0,z_0)=A_0(\xi_0)\mathrm{e}^{-\beta_0 z_0}, \quad \beta_0=\sqrt{\xi_0^2-k_0^2} \tag{18}$$

where $A_0(\xi_0)$ must be determined from the boundary conditions, and the term β_0 contains the information on the material properties. The boundary conditions in Eqs. 10 and 11 can be now expressed also using Hankel transform and dimensionless quantities:

$$u_0(r_0,0)=\mathbf{H}_1[\bar{u}(\xi_0,0);r_0]=\theta_0 r_0, \quad 0<r_0\le 1 \tag{19}$$

$$\tau_{0\varphi z}(r_0,0)=\mathbf{H}_1\left[\frac{\mathrm{d}\bar{u}(\xi_0,0)}{\mathrm{d}z_0};r_0\right]=0, \quad r_0>1 \tag{20}$$

Substituting the general solution of Eq. 18 in Eqs. 19 and 20, the following pair of dual integral equations describes the problem:

$$\mathbf{H}_1[A_0(\xi_0);r_0]=\theta_0 r_0, \quad 0<r_0\le 1 \tag{21}$$

$$\mathbf{H}_1[-\beta_0 A_0(\xi_0);r_0]=0, \quad r_0>1 \tag{22}$$

The solution $A_0(\xi_0)$ of the integral Eqs. 21 and 22 can be found, as proposed by Gladwell (1980), introducing a new function $\Psi_0(x_0)$, using the Fourier sine transform $\mathbf{F}_s$:

$$\Psi_0(x_0)=\begin{cases}\mathbf{F}_s[\beta_0 A_0(\xi_0),x_0] & x_0\le 1\\ 0 & x_0>1\end{cases} \tag{23}$$

$$\mathbf{F}_s[f(t);x]=\sqrt{\frac{2}{\pi}}\int_0^\infty f(t)\sin(xt)\mathrm{d}t \tag{24}$$

The problem of a torsional vibrating source on a viscoelastic half space, for the case of a linear displacement field in the contact area, is then reduced to the following set of Fredholm integral equations of the second kind (Gladwell 1980):

$$\sqrt{\frac{2}{\pi}}\theta_0 x_0=\Psi_0(x_0)+\int_0^1 \Psi_0(x_0)M_0(x_0,y_0)\mathrm{d}y_0 \tag{25}$$

$$M_0(x_0,y_0)=\frac{2}{\pi}\int_0^\infty\left[\frac{\xi_0}{\sqrt{\xi_0^2-k_0^2}}-1\right]\sin(\xi_0 y_0)\sin(\xi_0 x_0)\mathrm{d}\xi_0 \tag{26}$$

Equations 25 and 26 can be solved representing the unknown function $\Psi_0(x_0)$ as a finite series of normalized Legendre Polynomials (Dorn 1980). Once $\Psi_0(x_0)$ has been determined, $A_0(\xi_0)$ is found using inverse Fourier sine transform. From the Hankel-transformed displacement of Eq. 18, the displacement in the entire half space is finally obtained by integration:

$$\begin{aligned}u_0(r_0,z_0)&=\mathbf{H}_1[\bar{u}_0(\xi_0,z_0);r_0]\\&=\int_0^\infty A_0(\xi_0)\xi_0\mathrm{e}^{-\sqrt{\xi_0^2-k_0^2}z_0}\mathbf{J}_1(\xi_0 r_0)\mathrm{d}\xi_0\end{aligned} \tag{27}$$

The dimensionless stress in the contact area can be determined from $\Psi_0(x_0)$ as

$$\tau_{0\varphi z}(r_0,0)=-\mathbf{H}_1[\mathbf{F}_s[\Psi_0(x_0);\xi_0];r_0] \tag{28}$$

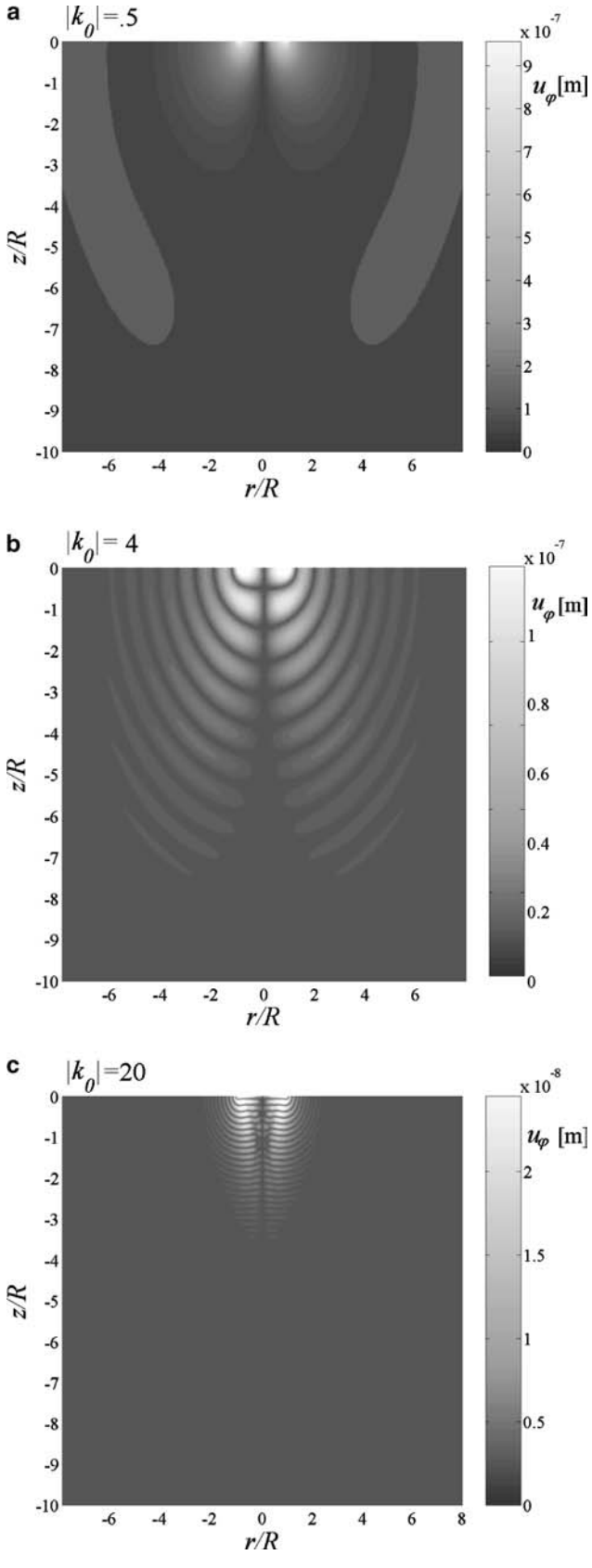

Fig. 6 Example of wave propagation patterns: amplitude of u_φ with $|k_0| = 0.5$, 4 and 20, respectively, and $\delta = 0.1$. Calculations for 1,300 Hz

The torsional radiation pattern and the torsional mechanical impedance of the medium can be determined for given values of the material parameters G_1 and G_2 for each excitation frequency. Calculations were performed using *Matlab* (The MathWorks). In Fig. 6, three examples of the radiation pattern generated by a torsional vibrating source are shown. Colors indicate the amplitude of the azimuthal displacement. The radiation pattern depends on the complex shear velocity c_{SH}, the exciting angular frequency ω and the radius of the contact area R, which define the dimensionless complex wave number k_0

$$k_0 = \frac{\omega}{\sqrt{G^*/\rho}} R = \left(\frac{\omega}{\sqrt{|G^*|/\rho}} R \right) e^{-j\frac{\delta}{2}} = |k_0| e^{-j\frac{\delta}{2}} \tag{29}$$

where the exponential notation for G^* has been used.

This number characterizes the wave propagation pattern. For stiff materials at low frequencies, wave propagation in radial direction is observed (Fig. 6a, where $|k_0| = 0.5$) . For soft tissues and relatively high frequencies, $|k_0|$ assumes values higher than 3, leading to waves propagating mainly in z-directions, toward tissue interior (Fig. 6b, with $|k_0| = 4$, and Fig. 6c, with $|k_0| = 20$). The attenuation of the SH waves within the half space is determined also by the phase angle δ of the complex shear modulus. The plots in Fig. 6 correspond to $\delta = 0.1$. Typically, stronger viscous components characterize the response of biological tissue, so that the amplitude of displacement decreases by one order of magnitude outside a layer of 3 to 4 times the oscillator

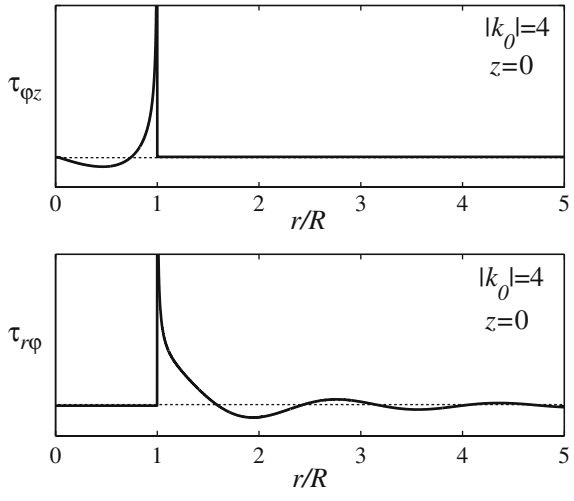

Fig. 7 Calculated shear stresses at $z = 0$ for a medium with $|k_0| = 4$, $\delta = 0.1$ at 1,300 Hz

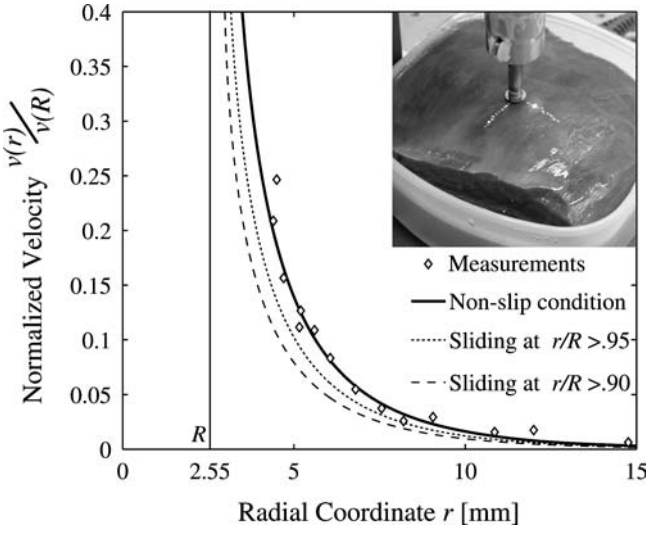

Fig. 8 Velocity field measured on the surface of a bovine liver sample with laser interferometry (experiment shown above right). Measurements are compared with the prediction of the analytical model assuming non-slip condition, sliding for the region $0.9 < r/R < 1$ and sliding for $0.95 < r/R < 1$

diameter $2R$. Therefore, the half-space model can be used for samples, in which the distance between radiating source and sample boundaries are in the range of 1–2 cm.

Figure 7 shows the components $\tau_{\varphi z}$ and $\tau_{\varphi r}$ of the stress vector at the tissue surface ($z = 0$) for a calculation with $|k_0| = 4$. The analytical solution leads to a stress singularity in correspondence of the external limit of the contact region $r \rightarrow R$. Sliding in the contact region must be prevented in order to reproduce in the experiment the boundary conditions assumed for the analytical model. The vacuum clamping adopted in the TRD device was designed to fulfill this condition. Measurements of the velocity field at the surface of a biological tissue sample were carried out in the vicinity of the resonator in order to verify the reliability of the non-slip assumption. Retro-reflecting spheres were distributed on the sample surface and the azimuthal velocity field determined by laser interferometry. Figure 8 shows that the velocity field predicted using the analytical model (with non-slip condition) agrees to a great extent with the measured values, whereas significant deviations are found with respect to a calculation assuming free sliding for the region $0.9 < r/R < 1$ and $0.95 < r/R < 1$. These results support the validity of the model assumption.

Interaction with the resonator and parameter extraction

By solving the analytical problem, the torque exerted by the soft tissue on the resonator can be expressed as a function of the material parameters. We assume that the density ρ of the tissue is known. Thus, the changes in the dynamic behavior of the resonator (the increase in damping and the resonance frequency shift) can be linked to the viscoelastic properties of the tissue. This is obtained by evaluating the complex transfer function of a torsional resonator, clamped at one end and subjected to the calculated torque from the soft tissue at the other end. The relationship between the material parameters G_1, G_2 and the measured parameters Q and Δf_{res} is determined. Figures 9 and 10 exhibit these relationships for the first resonance frequency. The mapping process allows obtaining the mechanical parameters of the tissue sample almost on-line.

Characterization of synthetic materials

The TRD technique has been applied for testing synthetic material. The main purpose of these experiments was to analyze the repeatability and assess the reliability

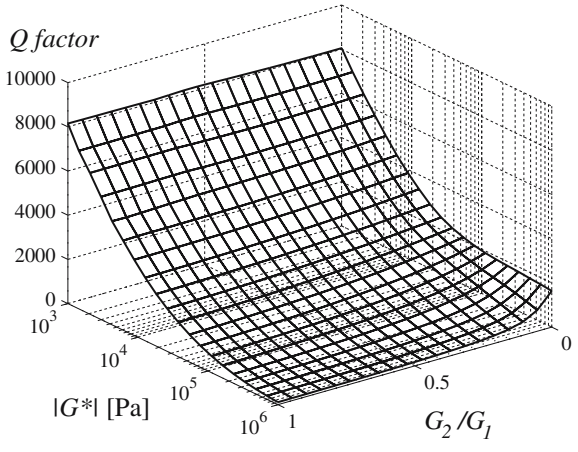

Fig. 9 Quality factor in function of G^* for the first resonance frequency (1,300 Hz)

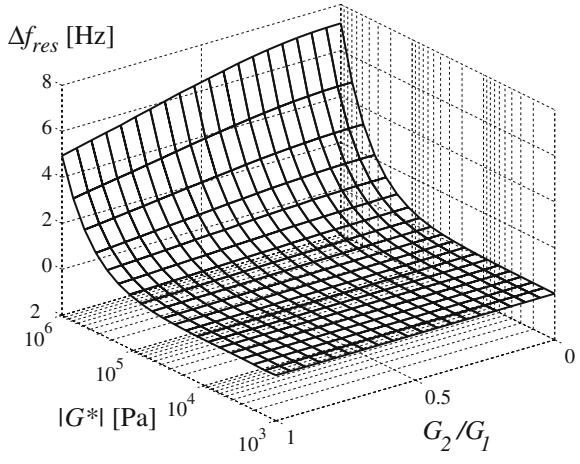

Fig. 10 Resonance frequency shift in function of G^* for the first resonance frequency (1,300 Hz)

Table 1 Synthetic materials

Sample	Material	Manufacturer	Density [g/cm^3]
Elastomer	UK-IIHC/20 ShA	Kundert	1.2
Silicone 3070	RTV6166 two-parts silicone gel 30%A 70%B	GE silicones	0.98

of the proposed method. To this end, the viscoelastic properties determined from the TRD tests are compared with the results obtained with wave propagation experiments on rod-like samples.

The materials used for these tests and their main characteristics are reported in Table 1. We have analyzed a relatively soft elastomer and a silicone with stiffness properties similar to those of soft biological tissues. The silicone used here has been previously investigated (Ottensmeyer 2002; Kalanovic et al. 2003) at lower frequencies (up to 10 Hz).

TRD tests

A cube specimen (side length: 60 mm) was available for testing the elastomer and a cylindrical specimen (diameter 60 mm, height 60 mm) for the silicone. The TRD device has been placed in the center of a flat face. Laser interferometer measurements were performed during the experiments at the other faces of the specimen and no displacements could be detected. This was expected, due to the relatively high-loss factors of these materials. This confirms that these testpieces can be modeled as a semi-infinite medium.

The tests with the TRD were conducted according to the procedure described above. The repeatability of TRD measurements have been investigated with multiple tests on the same testpiece. The results for the tests at the first resonance frequency (1,300 Hz) on the elastomer are reported in Fig. 11, which shows the measured values of Q and Δf_{res}. Measurements were repeated three times in four different locations, identified by the letters A, B, C and D. The material is assumed to be homogeneous so that the scatter is evaluated from the results of all locations. The resulting standard deviation for Q and Δf_{res} are 0.8% and 1.3% of the respective mean values, leading to the scatter of the calculated values of $|G^*|$ and G_2/G_1 shown in Fig. 12, that correspond to a Gauss distribution with standard deviation σ of 1.1% and 1.0%, respectively. Similar results in terms of standard deviations were obtained with the elastomer sample at the other frequencies. Standard deviations of up to 2% were obtained for $|G^*|$ and G_2/G_1 when testing the silicone sample.

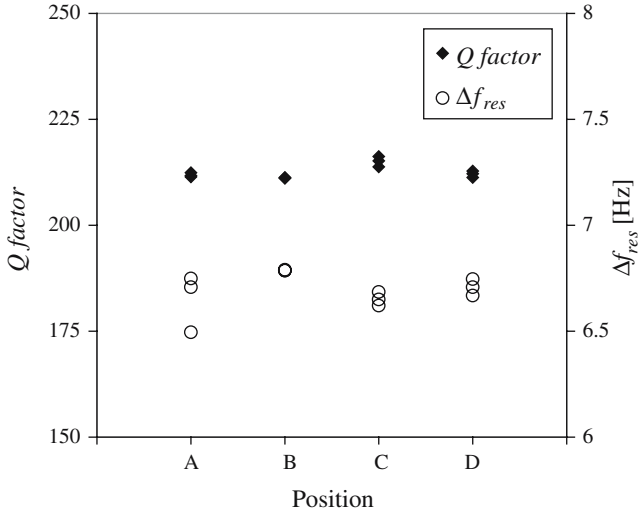

Fig. 11 Repeatability test on elastomer (1,300 Hz). Results for multiple tests on different locations (A, B, C, D) are reported

Wave propagation tests

The viscoelastic properties of the synthetic materials have been measured with an alternative method for comparison with the TRD technique. Standard rheometer or quasi-static uniaxial tests cannot be used for this purpose since the strain rate in these tests is in a much lower frequency range with respect to TRD. In order to achieve higher testing frequencies wave propagation experiments have been performed on rod-like testpieces of elastomer and silicone.

The time of flight of longitudinal waves were measured along the axis of samples with a squared cross section of 9×9 mm^2 and a length of 50 mm. The elastomer sample was directly extracted from the cube specimen used for the TRD experiments, while the silicone one was prepared with a mold. The experimental set-up is shown in Fig. 13. A piezo-transducer (Ferroperm, Pz27) was glued at one extremity of the bar and was used to excite longitudinal wave pulses. Displacement due to lateral contraction was measured with a laser interferometer (Polytec OVF5000): for this purpose, the lateral surfaces of the sample have been painted with reflecting color. The laser beam was placed at different points along the sample axis using a positioning system (Newport, IMS600) with high resolution (unidirectional repeatability 1.25 μm).

The real part of the complex longitudinal modulus, the storage modulus E_1, can be determined from the

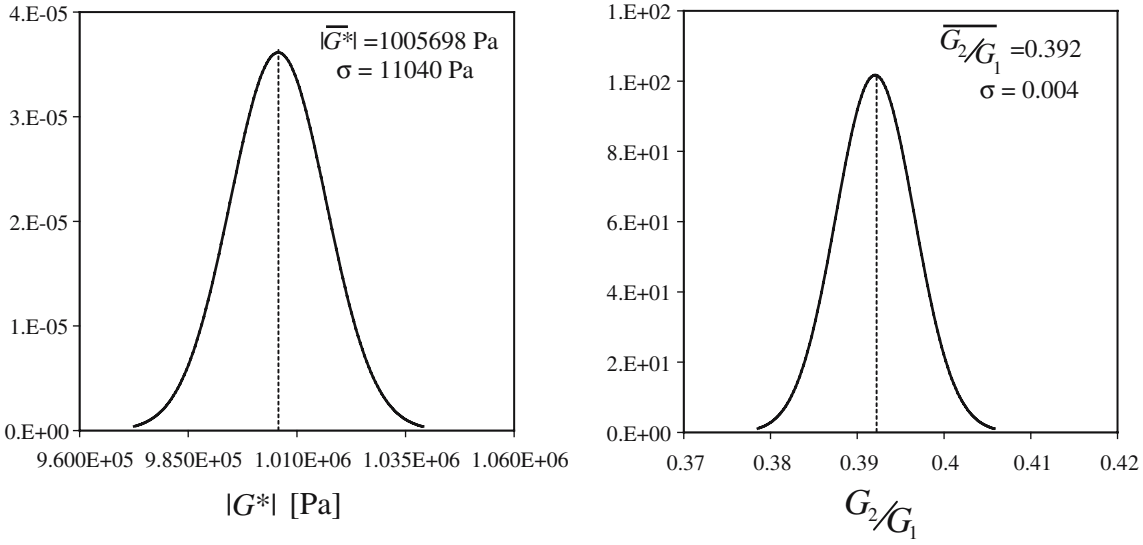

Fig. 12 Gaussian distribution of $|G^*|$ and G_2/G_1 from the data of Fig. 11. $|\overline{G^*}|$ and $\overline{G_2/G_1}$ indicate mean values and σ is the corresponding standard deviation

measured wave propagation velocity. The information on the loss angle δ (or, equivalently, on the loss modulus E_2) has to be inferred from an evaluation of the amplitude decay of the wave pulse along the sample. The quality of the measured displacement signals however did not allow quantifying the displacement amplitude with sufficient precision, so that the loss angle δ could not be measured.

Narrow band longitudinal wave pulses were excited in the bar at different frequencies. For the evaluation at higher frequencies (small wave length) corrections from the lateral contraction have to be considered in the relationship between longitudinal wave speed and E_1 (Graf 1991). The structural (longitudinal) wave model is not valid for ratio of wavelength to lateral dimension (polar radius of inertia of the cross section) smaller than 1. For the materials and the samples considered here this limitation leads to an upper limit for the frequency of approximately 3,500 Hz for the elastomer and 1,500 Hz for the silicone. This frequency range allows comparing results for the first resonance frequency of the TRD tests. Results for the elastomer and silicone are reported in Figs. 14 and 15. In order to validate the results at higher frequencies, the lateral dimensions of the rod sample should be reduced, this being very difficult due to the handling and manufacturing problems, in particular for the silicone beams.

With the elastomer rod sample the first two longitudinal resonance modes were excited using a harmonic

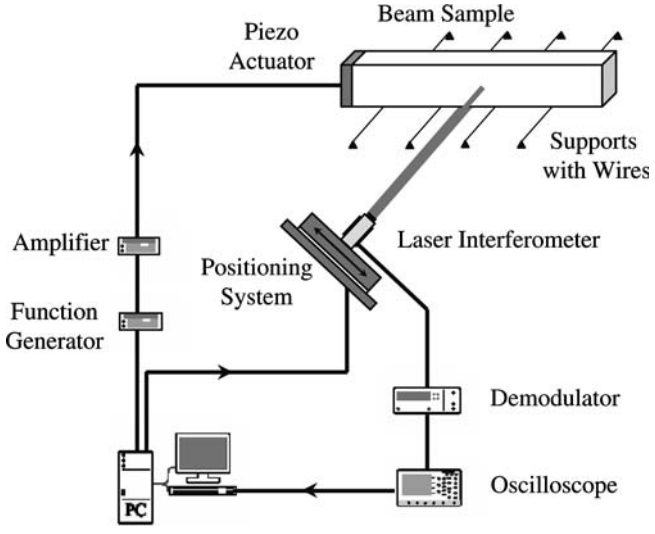

Fig. 13 Set-up for wave propagation experiments with a rod-like sample of synthetic material

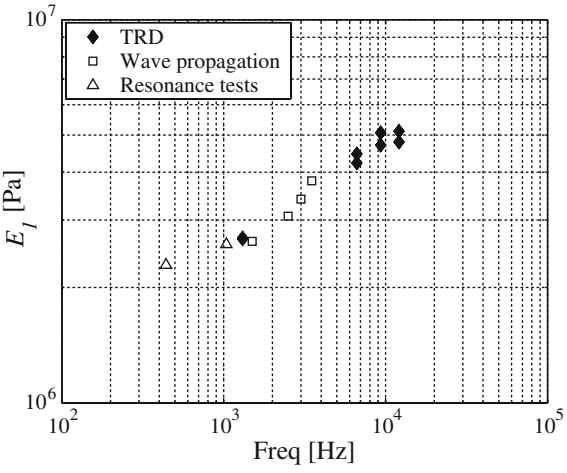

Fig. 14 Characterization of the elastomer: comparison between results obtained with wave propagation, resonance tests, and TRD

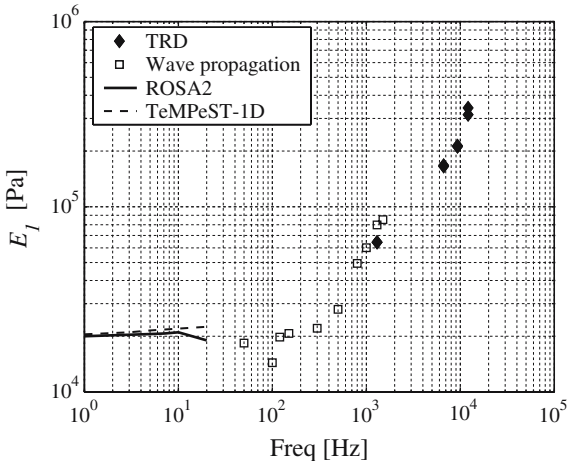

Fig. 15 Characterization of the silicone: comparison between results obtained with wave propagation and TRD. Low-frequency results obtained with the devices *ROSA*−2 and *TeMPeST*−1*D* by Kalanovic et al.(2003) are reported

signal. Higher resonance modes could not be excited, due to high damping. The viscoelastic moduli of the elastomer sample were extracted for the measured resonance frequencies and the corresponding values are reported in Fig. 14. No resonances were detected with the silicone sample due to the high-material damping.

Comparison

From the wave propagation tests the longitudinal storage modulus E_1 have been determined. Incompressibility has been assumed for these materials (Treloar 2005), $v = 0.5$, leading to

$$G_1 = \frac{E_1}{2(1+v)} = \frac{E_1}{3} \tag{30}$$

With this equation the corresponding values of E_1 were calculated from the TRD measurements of G_1 to enable a direct comparison with the wave propagation experiments, shown in Figs. 14 and 15. An increasing trend of E_1 with frequency is shown from the results of both techniques, while the values found on silicone at low frequency agree with the results in literature with the *ROSA*−2 and *TeMPeST*−1*D* devices by Kalanovic et al. (2003). For 1,300 Hz (the first resonance frequency of the TRD) the results agree to a great extent: the values differ by only 5% and 16% for the elastomer and silicone, respectively. Differences might be attributed to experimental errors, but the larger discrepancy for silicon might be caused by the fact that the sample was not extracted from the same specimen of the TRD tests but prepared in a subsequent step: although the silicon gel components were mixed in same proportion and according to the same procedure, slight differences in the gel composition cannot be excluded.

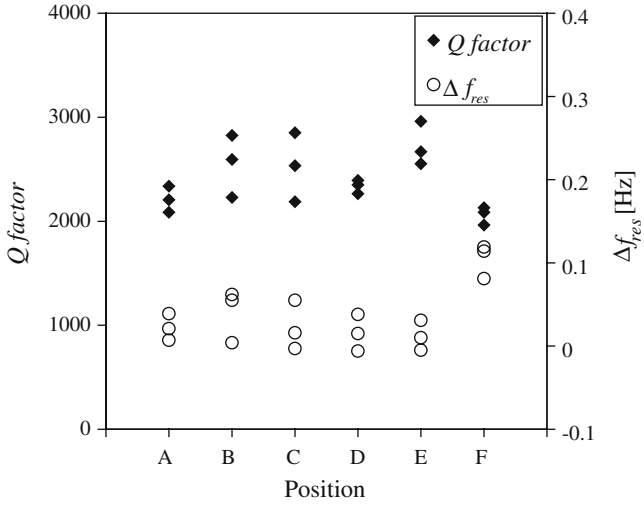

Fig. 16 Repeatability tests on bovine liver (capsule). Results for multiple tests at different locations (A–F) are reported

Characterization of soft biological tissue

The TRD technique was applied for testing bovine organs ex vivo. Adult bovine liver, kidney and uterus samples, obtained from the local abattoir, were tested at ambient temperature. In contrast to synthetic materials, soft tissues are inhomogeneous, can be composed of different layers (e.g., membranes which cover internal organs), are highly influenced by humidity (dehydration) and do not have a regular geometry. The consequences of these characteristics on the TRD experiments are analyzed with the present test series.

Repeatability

Figure 16 shows the results of the measurements on bovine liver in terms of Q and Δf_{res}. Measurements were performed at the external surface of the organ so that the TRD was in contact with the external membrane (called capsule) that covers the liver. The first TRD eigenfrequency (1,300 Hz) was considered in this analysis. A series of measurements were performed on the same organ at different locations, identified by the letters A, B, C, D, E, and F. Three measurements have been performed within short time intervals at each location.

Q factors are in the order of 2,400 with a standard deviation over all measurements of 12%. Very small variations are observed for the resonance frequency. As

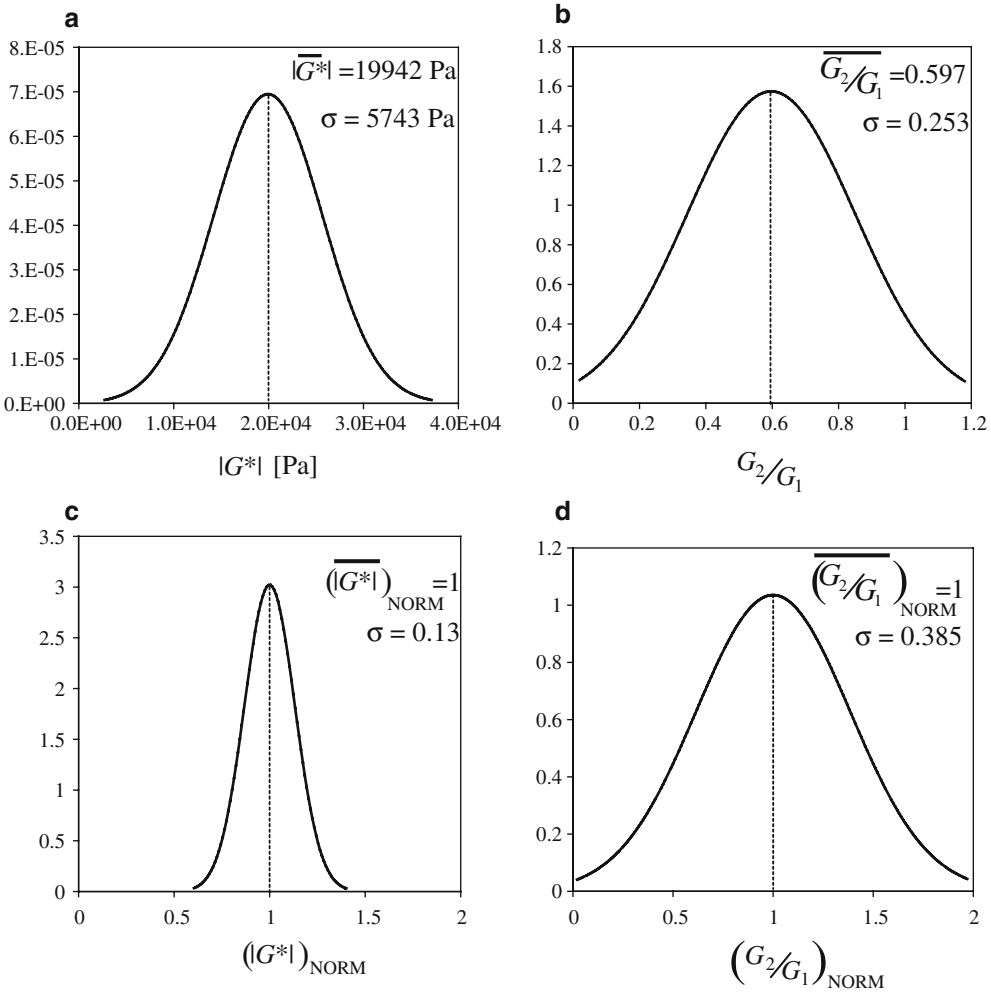

Fig. 17 **a–d** Gaussian distribution of $|G^*|$ and G_2/G_1, and point-normalized data $(|G^*|)_{\mathrm{NORM}}$ and $(G_2/G_1)_{\mathrm{NORM}}$ from the data of Fig. 16. Mean values and corresponding standard deviation σ are reported

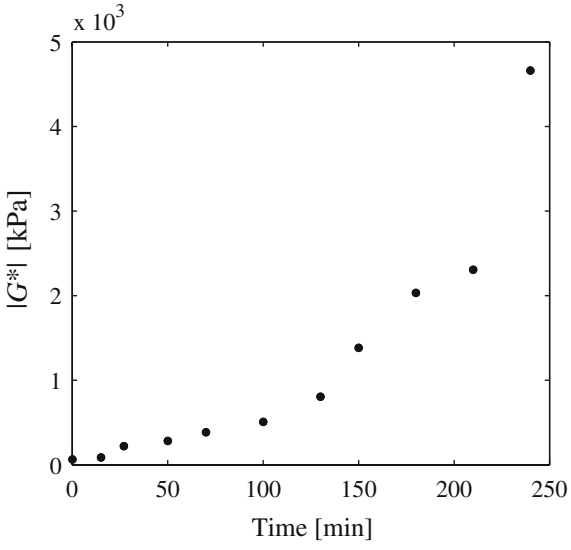

Fig. 18 Time evolution of $|G^*|$ on bovine liver (capsule) due to dehydration

a consequence, the standard deviation over all measurements is over 100% for Δf_{res}. The corresponding scatter of the calculated values of $|G^*|$ and G_2/G_1 is shown in Fig. 17a, b, that correspond to a Gauss distribution with standard deviation of 29 and 42%, respectively.

In order to eliminate variability from location to location, the $|G^*|$ and G_2/G_1 values of each location were normalized with respect to the location specific averages. The standard deviation of the normalized values $(|G^*|)_{\mathrm{NORM}}$ and $(G_2/G_1)_{\mathrm{NORM}}$ is 13% and 38%, respectively, leading to the distributions shown in Fig. 17c, d. This variability has to be attributed to the uncertainties of the experimental procedure and will be further discussed.

Figure 18 shows the time evolution of $|G^*|$ for TRD measurements performed at one single location at 1,300 Hz over a time range of 4 h. The organ was exposed to air in ambient conditions. The strong increase in stiffness is caused by tissue alterations due to dehydration and oxidation.

Table 2 TRD results on bovine organs at 1,300 Hz

Sample	$\overline{\lvert G^* \rvert}$ [Pa]	$\sigma_{\lvert G^* \rvert}$ [Pa]	$\overline{G_2/G_1}$	σ_{G_2/G_1}
Liver (capsule)	19,942	5,743	0.597	0.253
Liver (internal)	6,828	1,183	0.470	0.142
Kidney	6,767	1,076	0.484	0.113
Uterus	5,912	2,079	2.856	0.493

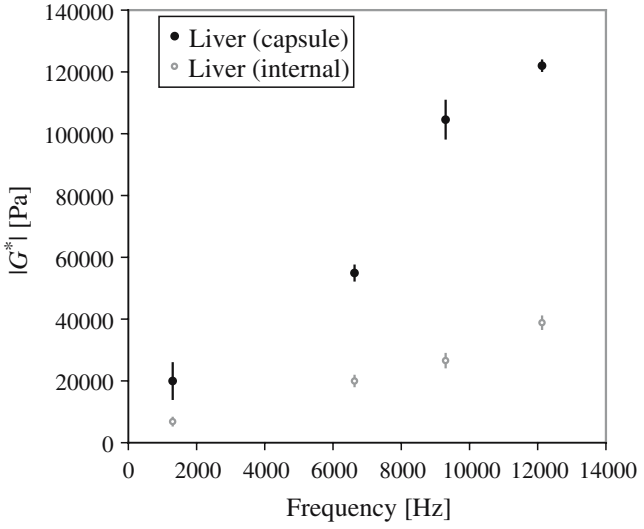

Fig. 19 TRD measurement results on bovine liver: capsule and internal liver section. Five tests were performed at different locations for each resonance frequency. The error bars correspond to an interval ± standard deviation

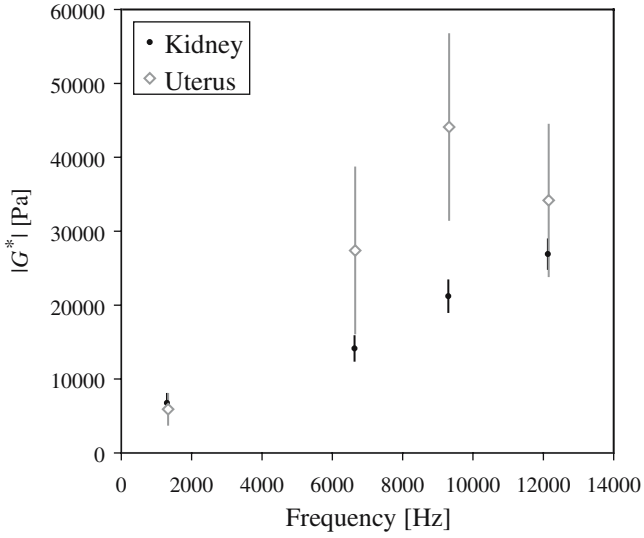

Fig. 20 TRD measurement results on bovine kidney and uterus. Five tests were performed at different locations for each resonance frequency. The error bars correspond to an interval ± standard deviation

Experiments with different bovine organs

In addition to liver capsule, liver interior (measurements at a sectioned surface), kidney, and uterus were investigated. Table 2 shows mean values and standard deviations of $|G^*|$ and G_2/G_1 obtained at 1,300 Hz. Five test (at five different locations) were performed on the same organ. Larger variability is observed for the uterus, which reflects the inhomogeneity of the organ. On the other hand, kidney show a relatively low scatter.

Frequency dependence

Performing experiments at the different eigenfrequencies of the resonator, the frequency dependence of the material behavior can be investigated. Results are reported for the first, the third, the fourth and the fifth TRD eigenfrequency. The second eigenfrequency of the torsional oscillator is very close to a bending mode so that excitation of a pure torsional vibration could not be achieved.

The measured values of the shear modulus $|G^*|$ on bovine liver are shown in Fig. 19, which includes the results for the liver capsule and for an internal section of liver. The comparison highlights the stiffening effect of the capsule. Five tests (at five different locations) were performed on the same organ and the corresponding variability is indicated in Fig. 19 by error bars, corresponding to an interval of $\pm\sigma$.

In Fig. 20, the results for kidney and uterus are reported. The larger scatter of uterus measurements is confirmed also at higher frequencies. Higher repeatability was observed when testing kidney.

Discussion

The reliability of the TRD experimental procedure and the analytical model are supported by the agreement of the results from TRD measurements and wave propagation experiments, as well as by the high repeatability of the TRD measurements with synthetic materials. A validation of the TRD method over a larger range of frequencies and material properties require dynamic experiments that are not easily performed with soft, highly damped materials. Several difficulties were

encountered when performing wave propagation experiments at high frequencies related to (1) sample preparation, (2) problems in handling very soft slender rod-like samples, (3) strong amplitude decay, in particular at high frequencies, leading to poor accuracy in displacement measurements. These problems highlighted the advantages of the TRD technique, for which no specific sample geometry is required, testing and data analysis is simple, fast and accurate, and rheological properties can be easily obtained for frequencies up to 10 kHz.

Multiple TRD experiments with synthetic materials with $|E^*|$ values larger than 100,000 Pa led to very high repeatability, with standard deviations as low as 1% with respect to the mean values of $|E^*|$ and E_2/E_1. The repeatability was significantly less in the experiments with soft biological tissue. The relatively large scatter obtained from measurements on liver at different locations (with standard deviation of 29% and 42% of the mean values of $|G^*|$ and G_2/G_1) is not surprising when compared to published experimental data on biological tissue (see e.g., Carter et al. (2001); Nava et al. (2004); Snedeker et al. (2005)). One important influential factor of this variability is the non-uniformity of the tissue, so that different responses are obtained at different locations in one organ. The results of Fig. 20, with significantly larger scatter for uterus, are related to larger non-uniformity of the uterus with respect to kidney.

The variability of the normalized $(|G^*|)_{\mathrm{NORM}}$ and $(G_2/G_1)_{\mathrm{NORM}}$ values for liver (Fig. 17c, d) however is due to the uncertainty of the experimental procedure. The corresponding standard deviations for $(|G^*|)_{\mathrm{NORM}}$ and $(G_2/G_1)_{\mathrm{NORM}}$, 13% and 38%, respectively, are relatively large. Larger variability of G_2/G_1 is due to the fact that both Q factor and Δf_{res} are more sensitive to variations in $|G^*|$ than to variations in G_2/G_1, see Figs. 9 and 10, so that uncertainties in Q factor and Δf_{res} have more influence on G_2/G_1.

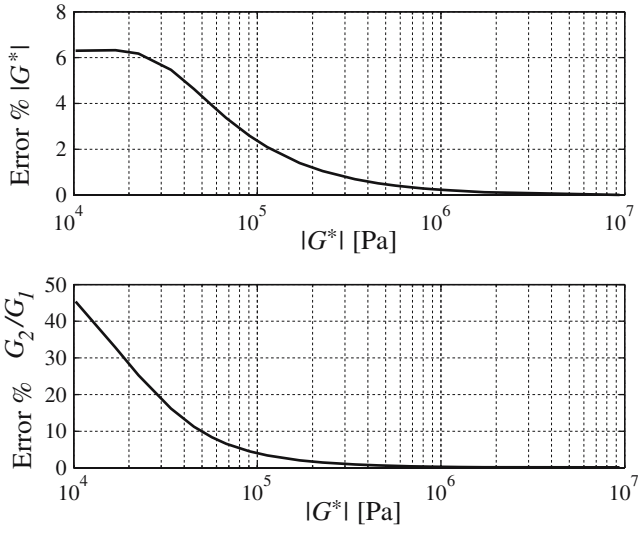

Fig. 21 Error evaluation on the parameters $|G^*|$ and G_2/G_1 due to an uncertainty of the resonance frequency measurement $\delta(\Delta f_{\mathrm{res}}) = \pm 0.02$ Hz. A value of $G_2/G_1 = 0.5$ has been assumed

Larger scatter in both $|G^*|$ and G_2/G_1 of liver with respect to synthetic materials can be mainly attributed to the uncertainties in the determination of Δf_{res}. As shown in Fig. 10, Δf_{res} values of less than 0.1 Hz are expected for a material with $|G^*|$ lower than 50,000 Pa (as for the liver). This means that the resonance frequency in calibration and measurement run has to be determined with very high accuracy.

The phase stabilization loop allows determining the resonance frequency with an accuracy of 10^{-6} in the present implementation (corresponding to about 0.001 Hz for the first TRD resonance frequency). The resonance frequency of the torsional resonator however is subjected to a larger variability, mainly due to the influence of temperature. At 1,300 Hz the standard deviation of a series of calibration runs (without contact with the tissue sample) is approximately 0.02 Hz. This variability corresponds to temperature fluctuations in the order of 0.1°C. Using the analytical model and assuming a material with $G_2/G_1 = 0.5$, the error in the determination of $|G^*|$ and G_2/G_1 due to a variation of Δf_{res} of ± 0.02 Hz can be calculated. The resulting errors are shown in Fig. 21 for different values of $|G^*|$. The curves show that: (1) the error in G_2/G_1 is always larger than the error in $|G^*|$; (2) for values of $|G^*|$ in the range of $10^5 - 10^6$ Pa (synthetic materials) errors are small; (3) errors increase with lower values of $|G^*|$. For $|G^*|$ in the range of 10^4 Pa (as in the case of liver) errors are in the range of 6% and 45% for $|G^*|$ and G_2/G_1, respectively. This error source represent therefore a significant contribution to the scatter of $(|G^*|)_{\mathrm{NORM}}$ and $(G_2/G_1)_{\mathrm{NORM}}$ obtained with the liver sample.

In addition to the above considerations, larger uncertainties affect the measurement when testing biological tissue with respect to synthetic materials, and are due to: (1) possible dependence of the mechanical response on the loading history (non-linear viscoelastic behavior); (2) the irregular shape of the sample surface which influences the contact area, with localized normal forces arising which are possibly not detected by the balance reading; (3) the tissue alterations due to dehydration leading to change of properties with time (see Fig. 18). The observed tissue alteration with time highlights the difficulties related to ex vivo biomechanical experiments, with the biological tissue changing its mechanical response when extracted from the natural biochemical environment.

The results of Figs. 19 and 20 show an increase of $|G^*|$ with frequency. This is in agreement with the results on soft internal organs described for lower frequencies by Nasseri et al.(2002), 0.01–10 Hz, by Kruse et al.

(2000) and Manduca et al.(2001), 50–300 Hz. Figure 19 allow comparing $|G^*|$ at the external surface with $|G^*|$ in the liver interior. The difference is significant and is due to the relatively stiff membrane (capsule), which influences to a great extent the results of the test.

As explained in Sect. 3, characterization of the rheological tissue properties can be obtained with the present technique only for homogeneous tissues. The measurements at the liver capsule could be used in combination with the characterization of the liver interior for determining the properties of the capsule. To this end, the analytical model is currently being extended to a two layer material (according to the procedure proposed by Dorn (1980)). The complex shear modulus of the capsule could be obtained from a combination of the results of surface and liver interior experiments.

Conclusions

A novel method has been proposed for determining the rheological properties of soft tissues in the frequency range 1–10 kHz. The procedure is fast (results for each frequency are obtained in approximately 1 min) and provides a local measurement, with a tissue volume of approximately 1 cm^3 influencing the outcome of the test. The complex shear modulus is determined from the experimental data with an analytical model.

First results for the validation of the proposed technique are provided by comparative measurements on synthetic materials. The results of tests on bovine organs demonstrate the suitability of the experimental procedure for characterization of biological tissues.

The repeatability tests have shown that high accuracy can be expected from experiments with materials in the range $|G^*| \sim 10^5$–10^6 Pa. Thus, this technique can be useful for characterizing soft polymers at frequencies up to 10 kHz with the advantage of simple and fast testing and data analysis.

Large scatter has been observed for biological tissue, being the stability of the resonance frequency the main error source. Future work will focus on possible reduction in the variability of the TRD resonance frequency. The resulting uncertainties in rheological properties, however, seem to be acceptable when compared to the scatter in the results of other testing methods and to the inherent variability of mechanical properties within soft organs.

Insight in the mechanical response of soft biological tissue is provided by the experiments presented here: (1) measured values of $|G^*|$ are in the range of 10^4–10^5 Pa; (2) for all organs $|G^*|$ increases with frequency; (3) the capsule has a significant stiffening effect on the mechanical response at the liver surface; (4) dehydration leads to significant changes in tissue rheological properties.

The TRD measurements results are used in our work for determination of constitutive models and, for this purpose, they are combined with quasi-static large deformation measurements with the aspiration device (see Nava et al. (2004)) leading to a characterization of the material behavior over a wide frequency range.

One significant limitation of the present experiment and analysis technique is represented by the fact that characterization of the rheological properties of biological or synthetic tissues can be obtained only for homogeneous and isotropic samples. An extension of the present modeling approach (using analytical and numerical methods) is currently being developed which will allow studying the influence of anisotropy and inhomogeneity on the interaction between sample and resonator.

Applications of the TRD technique in diagnostics will be explored in future work. No damage is caused by the experiment so that this method could be applied in vivo on human organs: during surgical interventions or organ inspections a local measurement of rheological properties could help distinguishing between healthy and unhealthy tissue. Current developments toward in vivo applications include: (1) a support and positioning system for the TRD device for use in the operation room; (2) a load cell to ensure zero normal force during measurements; (3) a computer algorithm for on-line extraction of viscoelastic parameters from the measured values of Δf_{res} and Q.

Acknowledgements This work was supported by the Swiss NSF project Computer Aided and Image Guided Medical Interventions (NCCR CO-ME). We thank the company Kundert AG, Jona, Switzerland, for providing the elastomer samples.

References

Abramowitz M, Stegun IA (1972) Handbook of mathematical functions with formulas, graphs, and mathematical tables. Dover Publications, New York

Arbogast KB, Thibaut KL, Scott Pinheiro B, Winey KI (1997) A high frequency shear device for testing soft biological tissues. J Biomech 30:757–759

Avis NJ (2000) Virtual environment technologies. Minim Invasive Ther 9:333–340

Bert CW (1973) Material damping: and introductory review of mathematical models, measures and experimental techniques. J Sound Vib 29:129–153

Bishop RED, Johnson DC (1979) The mechanics of vibration. Cambridge University Press, Cambridge

Carter FJ, Frank TG, Davies PJ, McLean D, Cuschieri A (2001) Measurement and modelling of the compliance of human and porcine organs. Med Image Anal 5:231–236

Dorn GA (1980) Radiation impedance and radiation patterns of torsionally vibrating seismic sources. PhD Thesis, University of California, Berkeley

Gladwell GML (1980) Contact problems in the classical theory of elasticity. Sijthoff and Noordhoff, Alphen aan den Rijn Germantown - Md

Graf KF (1991) Wave motion in elastic solids. Dover Publications, New York

Greenleaf JF, Fatemi M, Insana M (2003) Selected methods for imaging elastic properties of biological tissues. Annu Rev Biomed Eng 5:57–78

Hendriks FM, Brokken D, van Eemeren J, Oomens CWJ, Baaijens FPT, Horsten JBAM (2003) A numerical-experimental method to characterize the non-linear mechanical behaviour of human skin. Skin Res Tech 9:274–283

Kalanovic D, Ottensmeyer MP, Gross J, Gerhardt B, Dawson SL (2003) Independent testing of soft tissue viscoelasticity using indention and rotary shear deformation. Medicine Meets Virtual Reality, vol 11. IOS Press, pp 137–143

Kauer M, Vuskovic V, Dual J, Szekely G, Bajka M (2002) Inverse finite element characterization of soft tissues. Med Image Anal 6:275–287

Kruse SA, Smith JA, Lawrence AJ, Dresner MA, Manduca A, Greenleaf JF, Ehman RL (2000) Tissue characterization using magnetic resonance elastography: preliminary results. Phys Med Biol 45:1579–1590

Liu Z, Bilston LE (2000) On the viscoelastic character of liver tissue: experiments and modelling of the linear behavior. Biorheology 37:191–201

Manduca A, Oliphant TE, Dresner MA, Mahowald JL, Kruse SA, Amromin E, Felmlee JP, Greenleaf JF, Ehman RL (2001) Magnetic resonance elastography: non-invasive mapping of tissue elasticity. Med Image Anal 5:237–254

Miller K, Chinzei K, Orssengo G, Bednarz P (2000) Mechanical properties of brain tissue in vivo: experiment and computer simulation. J Biomech 33:1369–1376

Nasseri S, Bilston LE, Phan-Thien N (2002) Viscoelastic properties of pig kidney in shear, experimental results and modeling. Rheol Acta 41:180–192

Nava A, Valtorta D, Mazza E (2003) Experimental determination of the mechanical properties of soft biological tissues. In: Proceedings of the 9th international conference on the mechanical behaviour of materials, Geneva

Nava A, Mazza E, Kleinermann F, Avis NJ, McClure J, Bajka M (2004) Evaluation of the mechanical properties of human liver and kidney through aspiration experiments. Technol Health Care 12:269–280

Ottensmeyer MP (2002) TeMPeST 1-D: an instrument for measuring solid organ soft tissue Properties. Exp Tech 26:48–50

Picinbono G, Lombardo JC, Delingette H, Ayache N (2002) Improving realism of a surgery simulator: linear anisotropic elasticity, complex interactions and force extrapolation. J Visual Comp Animat 13:147–167

Robertson IA (1967) On a proposed determination of the shear modulus of an isotropic elastic half-space by forced torsional oscillations of a circular disc. Appl Sci Res 17:305–312

Romoscanu AI, Sayir MB, Häusler K, Burbidge AS (2003) High frequency parallel plate probe for the measurement of the complex viscosity of liquids. Rheol Acta 42:462–476

Sagoci HF (1944) Forced torsional oscillations of an elastic half-space II. J Appl Phys 15:655–662

Sayir M, Goodbread J, Häusler K, Dual J (1995) Method and device for measuring the characteristics of an oscillating system. Pat. Corp. Treat. PCT/EP95/00761

Sneddon IN (1966) The Reissner-Sagoci problem. Proc Glasgow Math Assoc 7:136–144

Snedeker JG, Bar-Bezat M, Niederer P, Schmidlin FR, Farshad M, Demetropoulos CK, Lee JB, Yang KH (2005) Strain-rate dependent material properties of the porcine and human kidney capsule. J Biomech 38:1011–1021

Szekely G (2003) Surgical simulators. Minim Invasive Ther 12:14–18

Treloar LRG (2005) Physics of rubber elasticity. Oxford University Press, Oxford

Zheng Y, Mak AFT (1996) An ultrasound indentation system for biomechanical properties assessment of soft tissues in vivo. IEEE Trans Biomed Eng 43:912–918